The detection of surface vibrations from interior acoustical pressure [*†]

Thomas DeLillo, Victor Isakov, Nicolas Valdivia, Lianju Wang

Abstract

We consider the problem of detecting the source of acoustical noise inside the cabin of a midsize aircraft from measurements of the acoustical pressure field inside the cabin. Mathematically this field satisfies the Helmholtz equation. In this paper we consider the three-dimensional case. We show that any regular solution of this equation admits a unique representation by a single layer potential, so that the problem is equivalent to the solution of a linear integral equation of the first kind. We study uniqueness of reconstruction and obtain a sharp stability estimate and convergence rates for some regularization algorithms when the domain is a sphere. We have developed a boundary element code to solve the integral equation. We report numerical results with this code applied to three geometries: a sphere, a cylinder with spherical endcaps, and a cylinder with a floor modeling the interior of an aircraft cabin. The exact test solution is given by a point source exterior to the surfaces with about 1% random noise added. Regularization methods using the truncated singular value decomposition with generalized cross validation and the conjugate gradient method with a stopping rule due to Hanke and Raus are compared. An interesting feature of the three dimensional problem is the relative insensitivity of the optimal regularization parameter (number of iterations) for the conjugate gradient method to the wavenumber and the multiplicity of the singular values of the integral operator.

1 Introduction

We consider the problem of identifying the source of the acoustical noise and the normal velocity of the sound on the surface of a three-dimensional domain Ω. The

[*]Supported by the NSF grant DMS 9803816 and NSF ITR/ACS grant 0081270 and the Cessna Aircraft Company.

[†]Department of Mathematics and Statistics, Wichita State University, Wichita, KS 67260-0033, U.S.A., E-mail: delillo@math.twsu.edu or victor.isakov@wichita.edu

acoustical field u of frequency k in Ω satisfies the Helmholtz equation

$$\Delta u + k^2 u = 0 \quad \text{in} \quad \Omega. \tag{1}$$

In our application Ω is the cabin of an aircraft. Microphones are located on a surface Γ_0 inside the cabin. They can measure the field u and the problem is to recover from these measurements u inside Ω and in particular

$$v = \partial_\nu u \quad \text{on} \quad \Gamma = \partial\Omega \tag{2}$$

which is the surface enclosing Ω. Here ν is the unit exterior normal to $\partial\Omega$. We will show that there is a unique representation of u by the single layer potential

$$u(x) = S\phi(x) := \int_\Gamma K(x,y)\phi(y)d\Gamma(y), \quad x \in \Omega \tag{3}$$

where

$$K(x,y) = \frac{e^{ik|x-y|}}{4\pi|x-y|} \tag{4}$$

is the free space radiating fundamental solution to the Helmholtz equation. This reduces our problem to solving the linear integral equation

$$\int_\Gamma K(x,y)\phi(y)d\Gamma(y) = \Phi(x), \quad x \in \Gamma_0 \tag{5}$$

where Φ is u measured on Γ_0. Given ϕ one can find the normal velocity from the formula

$$v(x) = D\phi(x) := \phi(x)/2 + \int_\Gamma \nabla_x K(x,y)\cdot\nu(x)\phi(y)d\Gamma(y), \quad x \in \Gamma \tag{6}$$

which follows from (3) and the jump relations for the normal derivative of single layer potentials. This approach in principle allows us to handle general domains Ω. Most existing methods either are based on the Helmholtz-Kirchhoff integral equation or are applicable to very special (rotationally symmetric Ω) where the Green's function of the Neumann problem for the Helmholtz equation can be found quite explicitly; see e.g. [16], [17]. Recently, Sean Wu suggested a very useful method based on approximation of a radiating solution by a family of special solutions which is applicable to any geometry. About a theoretical justification and applied results on this method we refer to the paper [12]. A review and theoretical foundation of the existing methods are given in [11].

In the paper ([4]) we considered a two-dimensional version of this problem. In this paper we consider the complete three-dimensional case.

In section 2 of this paper, we show that any $H_{(1)}(\Omega)$–solution to the Helmholtz equation (regardless of possible Dirichlet or Neumann eigenvalues) in a bounded Lipschitz domain Ω with connected complement can be uniquely represented by a single layer potential. When k^2 is not a Dirichlet or Neumann interior eigenvalue in Ω this result is known, but without these assumptions it is new. Section 3 contains stability estimates for recovery of u on Ω from u on Γ_0. As in ([4]) these conditional estimates are of Hoelder type inside of Ω and of logarithmic type in $\overline{\Omega}$. We attempt to find explicit formulae for the constants in the estimates for the particular case when Ω is the ball $|x| < r_1$ and Γ_0 is the sphere $|x| = r_0$. The obtained constants are rather sharp and the estimates show an increased stability with growing k. This increased stability was observed in many numerical papers on inverse scattering and it looks like a quite important phenomenon, but with the exception of continuation of solutions of the Helmhotlz equation across a plane there are almost no theoretical results about this increased stability. Obtaining corresponding stability estimates seems to be very difficult, by both advanced (Carleman estimates) and elementary (say, logarithmic stability) methods. So far it looks that the estimates of section 3 are the best available. Also we give convergence rates for the truncated singular value decomposition method. Section 4 reports the results of our numerical experiments.

Recall that $H_{(k)}(\Omega)$ denotes the Sobolev space of functions on Ω whose partial derivatives up to order k are square integrable and $\|\cdot\|_{(k)}$ denotes the standard norm in this space. We let $\|\cdot\|_2 = \|\cdot\|_{(0)}$ be the norm in the space $L^2(\Omega)$. Correspondingly, $|\cdot|_{l+\lambda}, 0 < \lambda < 1$ is the norm in the Hoelder space $C^{l+\lambda}$ of functions whose partial derivatives up to order l are Hoelder continuous with exponent λ.

2 Single layer potential representation.

We will characterize the source of an acoustical field $u(x)$ in $\Omega \subset \mathbb{R}^3$ by its surface density ϕ on $\partial\Omega$. In other words, for a solution u to (1) we would like to find a function ϕ such that (3) holds.

We will assume that $\partial\Omega \in Lip$ which means that $\partial\Omega$ is locally the graph of a Lipschitz function. We will consider only Ω with connected $\mathbf{R}^3 \setminus \overline{\Omega}$. In the following theorem we will use traces of functions in Sobolev spaces. These traces are well defined for C^∞-functions, moreover the corresponding trace operators ($u \to u$ on $\partial\Omega$ from $H_{(1)}(\Omega)$ into $H_{(\frac{1}{2})}(\partial\Omega)$ and $u \to \partial_\nu u$ on $\partial\Omega$ from $H_{(1)}(\Omega)$ into $H_{(-\frac{1}{2})}(\partial\Omega)$) are continuous, so the traces can be understood using approximation by smooth functions. The continuity of the mentioned operators follows from the known results on the solutions of the Dirichlet problem in $H_{(1)}(\Omega)$ ([15], p.226).

A possibility of the representation (3) is guaranteed by the following

Theorem 2.1 *For any solution $u \in H_{(1)}(\Omega)$ to the Helmholtz equation (1) there is an unique function $\phi \in H_{(-\frac{1}{2})}(\Gamma)$ such that (3) holds. Moreover, for some constant C depending only on Ω we have*

$$C^{-1}\|u\|_{(1)}(\Omega) \leq \|\phi\|_{(-\frac{1}{2})}(\Gamma) \leq C\|u\|_{(1)}(\Omega) \tag{7}$$

and if in addition $u \in C^{1+\lambda}(\overline{\Omega})$ and $\partial\Omega \in C^{1+\lambda}$, then

$$C^{-1}|u|_{1+\lambda}(\Omega) \leq |\phi|_\lambda \leq |u|_{1+\lambda}(\Omega) \tag{8}$$

Proof:

We first prove uniqueness of the representation (3). By the known properties of the single layer potential S with $H_{(-\frac{1}{2})}(\Gamma)$-density ϕ ([15], p. 203, Chapter 9) we have

$$-\Delta S_- - k^2 S_- = 0 \qquad \text{in } \Omega, \ -\Delta S_+ - k^2 S_+ = 0 \qquad \text{in } \mathbf{R}^3 \setminus \overline{\Omega},$$
$$S_- - S_+ = 0, \ \partial_\nu S_- - \partial_\nu S_+ = \phi \qquad \text{on } \Gamma \tag{9}$$

and the Sommerfeld radiation condition

$$\lim r(\partial_r S_+ - ikS_+)(x) = 0$$

as $r = |x|$ goes to infinity. Here S_- is S on Ω and S_+ is S outside Ω. To show uniqueness it suffices to assume that $S_=0$ on Ω and to derive that $\phi = 0$. If $S_- = 0$ on Ω, from the first jump relation we have $S_+ = 0$ on Γ. Then $S_+ \in H_{(1)}(B \setminus \Omega)$ (for any ball B) solves the homogeneous Helmholtz equation outside Ω, satisfies the homogeneous Dirichlet condition on Γ and the radiation condition at infinity. It is known ([15], pp. 286-289) that such $S_+ = 0$. Hence from the second of the jump relations (9) we conclude that $\phi = 0$.

Now we similarly will prove existence of ϕ. As mentioned above, there is the trace $g \in H_{(\frac{1}{2})}(\Gamma)$ of the function u on Γ and the trace operator from $H_{(1)}(\Omega)$ into $H_{(\frac{1}{2})}(\Gamma)$ is bounded. According to the cited elliptic theory ([15]) there is a unique radiating solution $u^+ \in H_{(1)}(B \setminus \Omega)$ to the Helmholtz equation in $\mathbf{R}^3 \setminus \overline{\Omega}$ with the Dirichlet data g on Γ. Here B is any ball in $\mathbf{R}^3$. As known ([15]) for the solutions u, u^+ of the interior and of the exterior Dirichlet problems in Ω with the Dirichlet data g there are traces $\partial_\nu u, \partial_\nu u^+ \in H_{(-\frac{1}{2})}(\Gamma)$ and the trace operator is continuous from $H_{(\frac{1}{2})}(\Gamma)$ into $H_{(-\frac{1}{2})}(\Gamma)$. Let $\phi = \partial_\nu u - \partial_\nu u^+$ on Γ. We claim that (3) holds.

Indeed, let S be the single layer potential $S\phi$ and U be the function defined as u on D and as the solution to the exterior Dirichlet problem with the data g on Γ outside Ω and with the radiation condition. Then S and U solve the same transmission problem (9) with the radiation condition at infinity.

A solution of this transmission problem is unique. This follows from the fact that a solution to a homogeneous problem ($\phi = 0$) solves the homogeneous Helmholtz equations in $\mathbf{R}^3$ and it satisfies the radiation condition. Hence it is zero. Indeed, when $\phi = 0$ by using the definition of a weak solution one can be convinced that S also solves the Helmholtz equation in $\mathbf{R}^3$ and satisfies the radiation condition. It is well known that then $S = 0$. By the uniqueness in the transmission problem we conclude that $S = U$.

The bounds (7) follow from the known results ([15]) on solvability of the Dirichlet problem in Lipschitz domains and from the continuity properties of layer potentials in these domains. In particular, we use the fact that the Dirichlet-to-Neumann operator mapping the Dirichlet data u on $\partial\Omega$ for the Helmholtz equation into the Neumann data $\partial_\nu u$ on $\partial\Omega$ is bounded from $H_{(\frac{1}{2})}(\partial\Omega)$ into $H_{(-\frac{1}{2})}(\partial\Omega)$.

The bounds (8) can be proven similarly, when we replace Sobolev space by Hoelder space and use known regularity properties of potentials and solutions to elliptic boundary value problems in these spaces collected for example in ([9]), section 1.6.

The proof is complete.

The above idea of the proof was suggested by John Sylvester (for smooth u, Ω) while discussing the representation by single layer potential obtained in the paper ([4]). While the proof of ([4]) most likely is valid for Theorem 2.1, we found that the Sylvester's idea combined with the available elliptic theory ([15]) is easier to implement for Lipschitz domains.

3 Uniqueness and stability for the inverse source problem

In this section we will derive sharp stability estimates for our inverse problem and give convergence rates for the truncated singular value decomposition method when Ω is the unit sphere. The uniqueness and stability problem is naturally decomposed into the (well-posed) Dirichlet problem for the Helmholtz equation in the domain Ω_0 bounded by Γ_0 and the problem of the continuation of a solution to this equation from Ω_0 onto Ω. The Dirichlet problem however can have eigenvalues (in particular for our specific application) which are relatively easy to find for spherical Ω and to bound from above and below for more general domains by using monotonicity of Dirichlet eigenvalues with respect to a domain. Nonuniqueness generated by these eigenvalues cannot be avoided. Away from them the Dirichlet problem is stable in classical Sobolev (or Hoelder) spaces. The problem of continuation of solutions of elliptic equtions is notoriously unstable. However assuming that $\|u\|_2(\Omega) < M_0$ one has the conditional Hoelder type estimate

$$\|u\|_{(k)}(\Omega_1) < CM_0^{1-\mu}\|u\|_2^{\mu}(\Omega_0) \tag{10}$$

where C, μ depend on $\Omega, \Omega_0, k, 0 < \mu < 1$ and on the distance from $\Omega_1 \subset \Omega$ to $\partial\Omega$. We refer for proofs to ([10]), sections 3.2,3.3. More delicate stability estimates of $\|u\|_2(\Omega)$ need some further constraints, like the bound $\|\nabla u\|_2(\Omega) < M_1$ and then one can obtain logarithmic conditional stability estimates

$$\|u\|_2(\Omega) \leq \frac{C}{|\log(\|u\|_2(\Omega_0))|^{\frac{1}{2}}} \tag{11}$$

where C depends on Ω, Ω_0, M_1, k. In applied situations the bounds M_0, M_1 (potential energy) can be available from physical nature of the problem. The stability estimates (10), (11) imply convergence rates for certain regularization algorithms of numerical solution. However, in the general situation it is very hard to obtain explicit bounds for C, μ. In this section we will obtain rather sharp bounds for these constants when $\Omega = \Omega(r_1)$, $\Omega_0 = \Omega(r_0)$. Here $\Omega(r)$ is the ball $|x| < r$.

Theorem 3.1 *Let u be a solution to the Helmholtz equation (1) in the ball $\Omega(r_1)$ and*

$$\|u\|_2(\Omega(r_1)) \leq M_0, \|\nabla u\|_2(\Omega(r_1)) \leq M_1. \tag{12}$$

Then

$$\frac{r_0^3}{r^2}\|u\|_2^2(\partial\Omega(r)) \leq C_1(r)\varepsilon_0^2 + C_2\varepsilon_1^{2\mu}, \quad r < r_1 \tag{13}$$

where $\varepsilon_0^2 + \varepsilon_1^2 = \|u\|_2^2(\partial\Omega(r_0))$, $C_1(r) = \max|\frac{j_n(kr)}{j_n(kr_0)}|^2$ *over* $n \leq n_1, n_1 = \frac{k^2r_1^2-3}{2}$, $C_2 = 5M^2$, $M^2 = 4M_0^2 + r_1^2M_1^2$, $\mu = \frac{\ln r_1 - \ln r}{\ln r_1 - \ln r_0}$.

In addition,

$$\|u\|_2^2(\partial\Omega(r_1)) \leq C_1(r_1)\varepsilon_0^2 + C_3\varepsilon_2(C_4 - \ln\varepsilon_2) \tag{14}$$

where $C_3 = \frac{1}{r_0}\max(k^2M_0^2, M_1^2)\ln\frac{r_1}{r_0}$, $\varepsilon_2 = -\frac{1}{\ln\frac{\varepsilon_1}{M}}$, *and* $C_4 = 1 - \ln\frac{r_0^3C_3}{5M^2}$.

In the proof we will use the following known expansion of a solution u to the equation ([3])

$$u(r,\theta) = \sum_{n=0,1,\ldots;-n\leq m\leq n} u_{n,m}j_n(kr)Y_{n,m}(\theta), \theta \in S^2 \tag{15}$$

where

$$j_n(t) = \sum_{p=0}^{\infty}\frac{(-1)^p}{p!1\cdot 3\cdot\ldots\cdot(2n+2p+1)}t^{n+2p}$$

is the n-th Bessel function and (r,θ) are the polar coordinates in the three-dimensional space and $Y_{m,n}$ are $L^2(S^2)$-orthonormal spherical harmonics. This expansion shows that nonuniqueness can occur only when the function $j_n(kr_0) = 0$ for some $n = 0, 1, 2, \ldots$

In addition we will make use of the following simple

Lemma 3.1 *Under the condition (12) we have*

$$\int_{|x|=r}|u|^2 \leq ((4r^{-1}M_0^2 + rM_1^2),\ -k^2M_0^2 \leq Re\int_{|x|=r}\partial_\nu u\overline{u} \leq M_1^2$$

provided $\Delta u + k^2u = 0$ *in* Ω.

Proof: ¿From the integration by parts formula in the polar coordinates we have

$$r\int_{|x|=r}u\overline{u} = \int_{|x|<r}r(\partial_r u\overline{u} + u\partial_r\overline{u}) + 3\int_{|x|<r}|u|^2 \leq$$

$$\leq \int_{|x|<r}(|u|^2 + r^2|\partial_r u|^2) + 3\int_{|x|<r}|u|^2 \leq \int_{|x|<r}(4|u|^2 + r^2|\nabla u|^2)$$

and by using (12) we have the first bound of lemma 3.1.

Again using integration by parts, we have

$$0 = \int_{|x|<r}(\Delta u + k^2u)\overline{u} = \int_{|x|=r}\partial_\nu u\overline{u} - \int_{|x|<r}(\nabla u\cdot\nabla\overline{u} - k^2u\overline{u})$$

and we similarly arrive at the second bound of this lemma.

The proof is complete.

Proof of Theorem 3.1: We let $t = kr$. Due to the choice of n_1 we have

$$j_n(t) = \frac{t^n}{1 \cdot 3 \cdot ... \cdot (2n+1)}(1 - \rho_n(t)) \tag{16}$$

where $|\rho_n(t)| < 0.55$ when $n_1 < n$. Indeed,

$$\rho_n(t) = \frac{t^2}{2(2n+3)}(1 - \frac{t^2}{22!(2n+5)} +$$

$$\sum_{p=1}^{\infty} \frac{1}{(2p+1)!(2n+5)...(2n+4p+3)}(1 - \frac{1}{(2p+2)(2n+4p+5)}\frac{t^2}{2})(\frac{t^2}{2})^{2p}) \leq$$

$$\frac{t^2}{2(2n+3)}(\frac{2}{3} + \frac{1}{3}\sum_{p=0}^{\infty}\frac{1}{(2p)!}(\frac{t^2}{2(2n+5)})^{2p}) \leq$$

$$\frac{t^2}{2(2n+3)}(\frac{2}{3} + \frac{e^{\frac{t^2}{2(2n+5)}} + e^{-\frac{t^2}{2(2n+5)}}}{6}) \leq \frac{t^2}{2(2n+3)}1.1$$

Here we used that, due to our choice of $n_1 \leq n$, we have $t^2 \leq 2n+3$ and that $e^{0.5} + e^{-0.5} \leq 2.25$. Similarly, $0 < \rho_n$.

Since the spherical harmonics are orthonormal in $L^2(S^2)$ we have from (15) that

$$\|u(t/k,)\|_2^2(S^2) = f_0(t) + f_1(t) \tag{17}$$

where

$$f_0(t) = \sum_{m \leq 2n+1, n < n_1} |u_{n,m}|^2 j_n^2(t) = \int_{|\theta|=1} |u(r,\theta)|^2 d\Gamma(\theta)$$

and f_1 is the similar sum over $n_1 \leq n$.

From the definition of f_0 and from the choice of C_1 we have

$$f_0(t) \leq C_1(r) f_0(t_0). \tag{18}$$

To obtain a bound for f_1 we will replace it by the simpler function

$$F(t) = \sum_{n_1 \leq n} \frac{|u_{n,m}|^2}{(1 \cdot 3 \cdot ... \cdot (2n+1))^2} t^{2n}.$$

¿From (16) and (17) it follows that

$$\frac{1}{5}F(t) \leq f_1(t) \leq F(t). \tag{19}$$

It is not hard to check that the function $h(s) = F(e^s)$, $s = \ln t$ is logarithmically convex: $h'^2 \leq h^{(2)}h$. Hence ([10], section 3.1)

$$h(s) \leq (h(s_0))^{\frac{s_1 - s}{s_1 - s_0}} (h(s_1))^{\frac{s - s_0}{s_1 - s_0}}$$

and using (19) twice yields

$$f_1(t) \leq F(t) \leq (F(t_0))^{\mu}(F(t_1))^{1-\mu} \leq 5(f_1(t_0))^{\mu}(f_1(t_1))^{1-\mu}$$

with $\mu = \frac{s_1-s}{s_1-s_0}$. Observing that

$$f_1(t) = r^{-2}\int_{|x|=r} |u_1|^2 \leq r^{-3}(4M_0^2 + r_1^2 M_1^2),$$

due to Lemma 3.1, we conclude that

$$f_1(t) \leq \frac{5}{r_0^3} M^{2-2\mu}\varepsilon_1^{2\mu},\ M^2 = 4M_0^2 + r_1 M_1^2. \tag{20}$$

Letting $\varepsilon_0^2 = r_0^2 f_0(t_0)$, $\varepsilon_1^2 = r_0^2 f_1(t_0)$ and using (18) we obtain the first (Hoelder) conditional stability estimate (13).

To obtain the logarithmic bound we will in addition make use of the second bound of Lemma 3.1. From (12) and (17) one can see that

$$|f_1'| = \frac{2}{kr^2}|Re\int_{|x|=r} \partial_\nu u_1 \overline{u}_1| \leq \frac{2}{kr^2}\max(k^2M_0^2, M_1^2)$$

By the Mean Value Theorem

$$f_1(e^{s_1}) = f_1(e^s) + f_1'(e^{s_2})e^{s_2}(s_1 - s) \leq A\varepsilon_{1*}^{2\mu} + B2\mu, \qquad \text{where } \varepsilon_{1*} = \frac{\varepsilon_1}{M}, s < s_2 < s_1.$$

Here we let

$$A = \frac{5M^2}{r_0^2},\ B = \frac{1}{r_0}\max(k^2M_0^2, M_1^2)\ln\frac{r_1}{r_0}$$

and we used (20). Minimizing $A\varepsilon_{1*}^{2\mu} + B2\mu$ we arrive at the value

$$\mu = \frac{\ln\frac{B}{A} - \ln(-\ln\varepsilon_{1*})}{2\ln\varepsilon_{1*}},\ \varepsilon_{1*}^{2\mu} = -\frac{B}{A\ln\varepsilon_{1*}}$$

and after substitution into the minimized expression we obtain (14).

In realistic cases, it should be possible to give numerical values for constants entering the conditional stability bounds of Theorem 3.1. In the two-dimensional case it is done in ([4]).

Now we will discuss the bound (14). As follows from the proof of Theorem 3.1, the space $L^2(S^2)$ is decomposed into the orthogonal sum of the spaces $H(0)$ and $H(1)$ spanned by the spherical harmonics $Y_{n,m}$ correspondingly with $n \leq n_1$ and $n_1 < n$. These spaces are invariant with respect to the operator of our problem. Accordingly, $u = u(0) + u(1)$, and the error in the data is split into ε_0 and ε_1. The bound (14) indicates that the problem in $H(0)$ is (Lipschitz) stable and strong (exponential) instability occurs only in $H(1)$. These stable and unstable parts of the solutions are called nonevanescent and evanescent waves ([16]). Since the space $H(0)$ is increasing when k is getting larger we expect better stability for greater k. This fact will be illustrated by our numerics in section 4.

Now we will study similar questions for the integral equation (5). We will consider $\Gamma = \{x : |x| = 1\}, \Gamma_0 = \{y : |y| = r\}$ and we let $\hat{x} = x/|x|$. We slightly modify the single-layer operator to $\hat{S} : L^2(\Gamma)$ into $L^2(\Gamma)$ by normalization $\hat{S}\phi(\hat{x}) = S\phi(x)$. The known addition theorem ([3], p. 29) gives

$$K(x, y) = ik \sum j_n(k|x|) Y_{n,m}(\hat{x}) h_n^{(1)}(k|y|) Y_{n,m}(\hat{y})$$

where the convergence is uniform provided $|x| < \theta|y|$ for some $\theta < 1$. Here and belwo the sums are over $n = 0, 1, ...; m = -n, ..., n$. Since the spherical harmonics form a complete orthonormal system in $L^2(\Gamma)$ we have the expansion $\phi(y) = \sum \phi_{n,m} Y_{n,m}(\hat{y})$. Hence

$$(\hat{S}\phi)(\hat{x}) = ik \sum j_n(kr) h_n^{(1)}(k) Y_{n,m}(\hat{x}) \int_\Gamma \phi(y) Y_{n,m}(\hat{y}) d\Gamma(y) =$$

$$ik \sum \phi_{n,m} j_n(kr) h_n^{(1)}(k) Y_{n,m}(\hat{x})$$

Summing up, $Y_{n,m}$ are singular functions of $\hat{S}$ with singular values

$$\sigma_n = |k j_n(kr) h_n^{(1)}(k)|.$$

The known asymptotics of the Bessel and Hankel functions ([3], p. 28) gives

$$\sigma_n = \frac{r^n}{2n+1}(1 + O(\frac{1}{n}))$$

as n goes to ∞.

We will show that

$$\sigma_n \geq \frac{r^n}{5(2n+1)} \tag{21}$$

provided $n_2 < n$ with $n_2 = \frac{3}{2}k^2 - 1$.

Indeed,

$$h_n^{(1)}(t) = j_n(t) + i y_n(t)$$

where

$$y_n(t) = -t^{-n-1} 1 \cdot 3 \cdot ... \cdot (2n-1)(1 - \rho_n(t))$$

with

$$|\rho_n(t)| = |\sum_{p=1}^{\infty} \frac{(-1)^p t^{2p}}{2^p p! (-2n+1)(-2n+3)...(-2n+2p-1)}| \leq$$

$$\frac{t^2}{2(2n-1)}(1 + \sum_{p=2}^{\infty} \frac{t^{2(p-1)}}{|4 \cdot ... \cdot 2p(-2n+3) \cdot ... \cdot (-2n+2p-1)|}).$$

Due to our restrictions, $\frac{t^2}{2(2n-1)} \leq \frac{1}{3}$. Observe that for integers p, n, $|2p(-2n+2p-1)| \geq 2n$. Pairing accordingly the terms in the denominator of the last sum, we obtain

$$|\rho_n(t)| \leq \frac{1}{3}(1 + \frac{1}{3} + \frac{1}{9} + ...) = \frac{1}{2}.$$

Now, using (16), we obtain

$$\sigma_n \geq |kj_n(kr)y_n(k)| \geq k\frac{(kr)^n}{1\cdot 3\cdot ...\cdot(2n+1)}0.45k^{-n-1}1\cdot 3\cdot ...\cdot(2n-1)0.5$$

which gives (21).

The truncated singular value decomposition (tsvd) for the equation (5) with the approximate right side Φ^δ ($\|\Phi^\delta - \Phi\|_2(\Gamma) \leq \delta$) provides the approximate solution

$$\phi_p^\delta = \sum_{n=0,...,p;m=-n,...,n} \frac{1}{\sigma_n}\Phi^\delta_{n,m}Y_{n,m}. \tag{22}$$

The purpose of the tsvd is to regularize the ill-posed problem (5) by cutting off higher harmonics generating exponential ill-conditioning. By using the bounds from the proof of Theorem 3.1 and (21) we will obtain a convergence rate for this regularization method when the exact solution ϕ to (5) satisfies the natural (smoothness) constraint

$$\sum n^2|\phi_{n,m}|^2 \leq M_1^2. \tag{23}$$

We have

$$\|\phi_p^\delta - \phi\|_2^2(\Gamma) =$$

$$\sum_{n\leq n_2}\frac{1}{|\sigma_n|^2}|\Phi^\delta_{n,m} - \Phi_{n,m}|^2 + \sum_{n_2<n\leq p}\frac{1}{|\sigma_n|^2}|\Phi^\delta_{n,m} - \Phi_{n,m}|^2 + \sum_{p<n}|\phi_{n,m}|^2 \leq$$

$$C_5\delta_0^2 + \frac{\delta_1^2}{|\sigma_p^2|} + \frac{M_1^2}{(p+1)^2}$$

where $\delta_0^2 = \sum_{n\leq n_2}|\Phi^\delta_{n,m} - \Phi_{n,m}|^2$, $\delta_1^2 = \delta^2 - \delta_0^2$, and $C_5 = \max\frac{1}{|\sigma_n|^2}$ over $n = 0, ..., n_2$ when we use the constraint (23). The first term of the last sum does not depend on p and it represents a (Lipschitz) stable part of our bound. The sum of the remaining terms in view of (21) does not exceed

$$\frac{100(p+1)^2}{r^{2p}}\delta_1^2 + \frac{M_1^2}{(p+1)^2}.$$

It is not hard to check that this function of p has a unique minimum point which gives an optimal value of the regularization parameter p (a stopping rule). However it is hard to find this minimum point analytically, so we let

$$p = \frac{\ln\delta_1}{2\ln r} \tag{24}$$

to conclude that $r^{2p} = \delta_1$ and the minimum is less than

$$100(\frac{\ln\delta_1}{2\ln r} + 1)^2\delta_1 + \frac{M_1^2}{(\frac{\ln\delta_1}{2\ln r}+1)^2}.$$

Summing up we have the convergence rate for the tsvd

$$\|\phi_p^\delta - \phi\|_2^2(\Gamma) \leq C_5\delta_0^2 + 100(\frac{\ln\delta_1}{2\ln r}+1)^2\delta_1 + \frac{M_1^2}{(\frac{\ln\delta_1}{2\ln r}+1)^2}$$

where $C_5 = \max \frac{1}{|kj_n(kr)h_n^{(1)}(k)|^2}$ over $n = 0, ..., n_2$ and $\delta^2 = \delta_0^2 + \delta_1^2$. As above the term with δ_0 contributes to the stable part of the bound while the remaining terms give a logarithmic conditional bound of the evanescent part of the solution.

4 Numerical solution of the integral equation (5) and regularization methods

In this section, we consider the numerical solution of the integral equation (5) for a range of wave numbers k. These investigations are similar to the two dimensional case [4], but with additional interesting features. We recall the setup. Here $k = \omega/c$, where ω denotes frequency and c is the speed of sound. In the case of interior aircraft cabin noise $c = 340m/sec$ and the range of interest of ω is typically in the range of human speech,

$$20\pi/sec < \omega = 2\pi f < 1000\pi/sec,$$

where f is frequency in Hertz. This leads to a *range of k* of

$$.06\pi/m < k < 3\pi/m.$$

Since cabin dimensions a are on the order of meters, the dimensionless quantity ka has a similar range.

Let S denote the single layer operator in (5) and D the Fredholm integral operator in (6). We have developed a Matlab code based on Atkinson's package [1], [2] using piecewise linear triangular boundary elements to produce N-node discretizations S_N and D_N of S and D over the boundary and measurement surfaces Γ and Γ_0. The numerical results reported below were run on a 500 MHz laptop.

Our numerical problem is the following: Given Φ on Γ_0, solve

$$S_N \phi = \Phi$$

for ϕ where we now let ϕ, Φ, and v denote N-vectors. In order to recover the normal velocities v (at the N nodes) on Γ, we then compute

$$v = D_N \phi.$$

For data Φ with measurement noise, it is necessary to regularize the solution to filter out high levels of noise in the high frequency modes associated with small singular values of S_N. The results developed in the previous sections of this paper guarantee the convergence of the regularized solution as the noise level goes to 0, in accordance with standard results from, e.g., [3], [5], [10], [14].

As in [4], we have tested a number of regularization and parameter selection routines described in [8], [6]. We will report on only a few repesentative calculations here using the truncated svd (tsvd in [7]) and the conjugate gradient method for the normal equations (cgls in [7]). In the case of the truncated svd, the regularization parameter p is the number of singular vectors retained in the reconstruction. More explicitly, we are solving the least squares problem

$$\min_{\phi} \|S_N \phi^\delta - \Phi^\delta\|_2$$

for ϕ^δ where $\Phi^\delta = \Phi + e$, $e =$ noise with $\|e\|_2/\|\Phi\|_2 = \delta$. To model the microphone noise in our numerical tests, we use normally distributed random noise with mean 0 and standard deviation 1 from the Matlab random number generator *randn* where $e = \delta\|\Phi\|_2 f/\|f\|_2$ with $f = \text{randn}(\text{size}(\Phi))$. The Matlab svd routine computes the singular value decomposition of our $N \times N$ matrix S_N:

$$S_N = U\Sigma V^*, \; U^*U = I, \; V^*V = I,$$

where $U = [u_1, \ldots, u_N]$, $V = [v_1, \ldots, v_N], \Sigma = diag(\sigma_1, \ldots, \sigma_N)$, and $\sigma_1 \geq \sigma_2 \geq \cdots \geq \sigma_N \geq 0$. The solution to least squares problem is then given by

$$\phi^\delta = \sum_{i=1}^{rank(S_N)} \frac{u_i^* \Phi}{\sigma_i} v_i + \sum_{i=1}^{rank(S_N)} \frac{u_i^* e}{\sigma_i} v_i.$$

The tsvd routine just truncates this solution after the first $p \leq N$ terms giving the regularized solution,

$$\phi_p^\delta = \sum_{i=1}^{p} \frac{u_i^* \Phi^\delta}{\sigma_i} v_i.$$

For conjugate gradient, the regularization parameter p is the number of conjugate gradient iterations. Since conjugate gradient for the normal equations minimizes the $S_N^* S_N$–norm error over the pth Krylov space $K_p(S_N^*\Phi^\delta, S_N^* S_N)$ and since

$$\|\phi - \phi_p^\delta\|_{S_N^* S_N}^2 = \|\Phi^\delta - S_N \phi_p^\delta\|_2^2,$$

at each step p conjugate gradient finds the least squares solution ϕ_p^δ over K_p. Our results below show that, as in the two dimensional case, the conjugate gradient method finds the optimal solution in the first several iterations and then diverges rapidly toward the solution to the problem with noisy data. This well-known semiconvergence behavior [6], [8] is due to the fact that conjugate gradient initially reduces the error in the direction of the dominant (low frequency) singular vectors v_i ($S^*Sv_i = \sigma_i^2 v_i$) which are less corrupted by noise relative to the high frequency modes corresponding to small σ_i. The choice of the regularization parameter p (stopping rule or spectral cutoff) is crucial.

In the examples below, we display two parameter choice methods: generalized cross validation (gcv in [7]) and the heuristic stopping rule for conjugate gradient given in [6], p. 51, Rule 3.13. The Hanke rule computes a value $c(p)$ for each step p of the conjugate gradient method. We plot $c(p)$ on the figures. An optimal p corresponds to a minimum of $c(p)$. If the noise level is known, the discrepancy principle [8] can be used. However, this is generally not the case in practice and we do not use that information here.

The number and location of the N values of Φ represent the number and location of the microphones. In practical engineering N may be on the order of 1000 uniformly distributed pressure measurements made by a moveable array of microphones. In our numerical experiments, the level of noise and number of microphones reflect this setup. The problem of the optimal number and placement of the microphones is a fundamental and difficult one, and we plan to address this issue in a future paper.

We now give results of our numerical calculations for three geometries and various values of k and δ to demonstrate the regularization techniques.

Our *relative errors* are given by

$$\|v - v_p\|_2/\|v\|_2 \leq \mathrm{cond}(\mathrm{D_N})\|\phi - \phi_p^\delta\|_2/\|\phi\|_2$$

where $v_p = D_N\phi_p^\delta$.

Example 1: Γ (the fuselage) is the unit sphere, Γ_0 (the microphone measurement surface) is the sphere of radius $r = .9$, and the exact Φ is a point source $\Phi(x, y, z) = e^{ikR}/R$ with $R = |(x, y, z) - (2, 0, 0)|$). The exact velocity v on Γ can be computed easily from Φ. The following table indicates how the relative errors in v_p for the optimal p (in parentheses in the tables), which we know from the exact v, changes for various noise levels δ. We see that as $\delta \to 0$ the relative error approaches 0, as expected from the theory. The condition numbers, $\mathrm{cond}(S_N)$ and $\mathrm{cond}(D_N)$, for each N are given in the 2-norm. D_N is well-conditioned, as expected, unless k is near an eigenvalue. (Unlike the direct problem, for the inverse problem k has to approximate an eigenvalue to several digits to have any noticeable effect on the numerical results.) $\sigma_1(S_N)$ is of order 1, so σ_N is of order $1/\mathrm{cond(S)}$. Note that for $\delta = 0$ the errors roughly decrease by a factor of 1/4 each time the surface triangulation is refined (sides halved) increasing N by approximately a factor of 4. This is the $O(h^2)$ behavior with $h = O(1/\sqrt{N})$ that one would expect with piecewise linear elements. Piecewise quadratic elements give better results for the noiseless examples, but unexpectedly lead to somewhat worse results for regularized solutions with 1% noise. Higher order methods do not appear to be advantageous for problems with high noise levels. The two dimensional results reported in [4] used the Nyström method, which is spectrally accurate for analytic curves and data. However, the regularized solutions for problems with 1% noise were not appreciably more accurate than the cases reported here.

Table 1 lists the optimal relative 2-norm errors using tsvd only at three noise levels and Table 3 compares optimal errors for tsvd and cg. Specifically, the value of p in the parentheses next to the error is the $p, 1 \leq p \leq N$, such that error $\|v - v_p\|_2/\|v\|_2$ is minimized. These values correspond to the minima of the error curves (for tsvd or cg) in Figures 1, 2, and 3, and they change very little for different random noise vectors e when δ is fixed. The Tables and Figures for Examples 2 and 3 are presented in a similar fashion. (The case $N = 2050, k = 1$ in Table 1 uses a few iterations of conjugate gradient and the Matlab condition number estimator, condest, were used, since the svd was very time consuming.) Note that it is necessary for the discretization error $O(h^2)$ for $(\delta = 0)$ to be on the order of the noise level δ in order to have any hope of recovering v.

k	N	cond(D_N)	cond(S_N)	$\delta = 0(p)$	.001	.01
1	66	1.7	$5.7 \cdot 10^1$	.11(66)	.11(66)	.22(66)
1	258	1.8	$3.9 \cdot 10^2$	.029(258)	.10(198)	.14(38)
1	1026	1.8	$8.6 \cdot 10^3$	.0073(1026)	.075(198)	.107(62)
1	2050	1.8	$8.7 \cdot 10^7$(est.)	.0077(100 cg)	.107(44 cg)	.19(13 cg)
3	66	5.8	$2.4 \cdot 10^1$	.17(66)	.17(66)	.20(66)
3	258	6.1	$1.8 \cdot 10^2$	.045(258)	.062(258)	.10(70)
3	1026	6.2	$4.1 \cdot 10^3$	.011(1026)	.052(350)	.071(98)
6	66	18.9	7.8	.35(61)	.35(61)	.35(61)
6	258	18.6	$8.9 \cdot 10^1$	.10(258)	.10(258)	.13(81)
6	1026	18.6	$2.2 \cdot 10^3$	.025(1026)	.049(346)	.063(150)

Table 1: Optimal relative errors for Example 1 (unit sphere with point source) achieved using (p) terms in tsvd at noise levels $\delta = 0, .001, .01$.

$\sigma_n(S_N)$	$\sigma_n(S) = \lvert k j_n(kr) h_n^{(1)}(k)\rvert$
0.88667725374117	0.87036323291943
0.39339630328749	0.39087804505651
0.18107791241820	0.18368536739401
0.10649046722208	0.11044706149441
...	...

Table 2: Comparison of some exact and computed singular values for Example 1.

Table 2 gives some sample computed and exact values of singular values $\sigma_n = |kj_n(kr)h_n^{(1)}(k)|, n = 0, 1, 2, 3$ of multiplicities $1, 3, 5, 7$, respectively, with $N = 258, k = 1$ and $r = 0.9$.

In Figures 1, 2, and 3, note that the optimal p for cgls appears to depend only slightly on k and hardly at all on the (odd) multiplicity of the singular values of S. This is in contrast to the truncated svd which requires $p = n^2$ terms if singular vectors associated with the first n distinct singular values are required, i.e. $\sigma_1/\sigma_n \approx \delta$. Conjugate gradient requires only one iteration per eigenspace. For the independence wrt k, we can use [13] Theorem 4.1, the fact that S is well-conditioned over the nonevanescent part of the spectra and that the tail of singular values of S decay asymptotically like r^j, independent of k. Similar behavior is observed for other typical geometries, as the next example illustrates. These interesting features make conjugate gradient methods particularly attractive and efficient for large scale acoustics problems.

Example 2: Γ (the fuselage) is a cylinder of length 3 and radius 1 with two hemispherical endcaps. Γ_0 (the microphone measurement surface) is the concentric cylinder of radius $r = .9$, and the exact u is a point source $u(x, y, z) = e^{ikr}/r$ with $r = |(x, y, z) - (0, 1.5, -0.5)|$). Table 3 lists the optimal relative error in the 2-norm

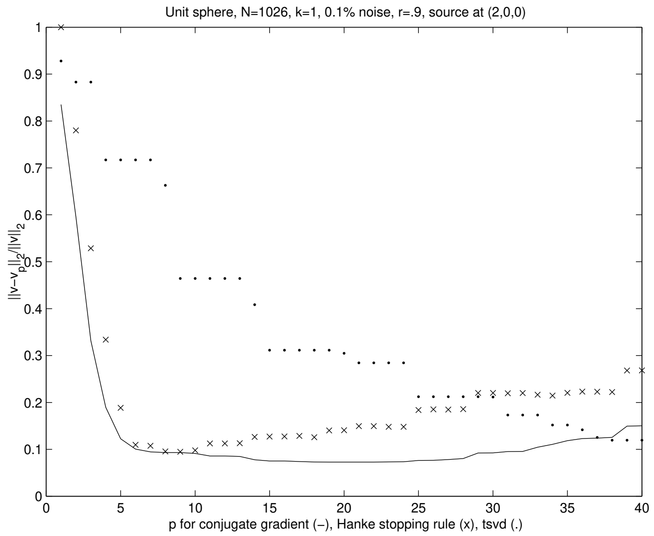

Figure 1.

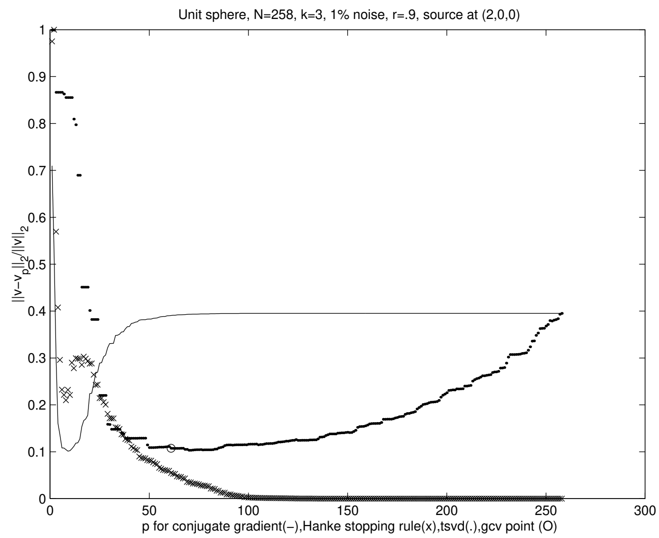

Figure 2.

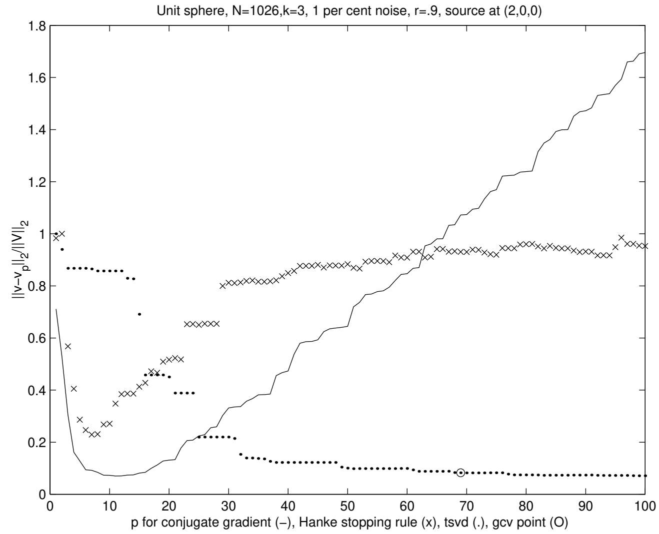

Figure 3.

and the p for which it was achieved for the truncated svd (tsvd) and the conjugate gradient (cg) methods. Figures 4 and 5 exhibit clearly that the behavior of tsvd and cg are qualitatively similar to the spherical geometry.

Example 3: Γ (the fuselage) is a cylinder of radius 1 and length 5 with flat endcaps and a floor at a distance .74 from the center. The boundary triangulation with 2048 boundary elements and 1026 nodes is shown in Figure 6. This geometry approximately models a Cessna 650 cylindrical fuselage with a floor. Table 4 lists the relative errors in the 2-norm for tsvd and cg. Table 5 lists the smallest average error in the 1-norm, $||v - v_p||_1/N$ and the value of p in parentheses where it occurs. This norm gives a better indication of the pointwise errors away from the corners and edges of the fuselage, where recovered velocities are not expected to be accurate. Figure 7 compares the semiconvergence and stopping rules for tsvd and cg. Table 6 gives timings in seconds for the numerical algorithm. Observe that the computation of S and D makes a major contribution to the cost and the computation of the svd becomes significant with increasing N. Exact and recovered velocity profiles are shown in Figures 8 and 9.

References

[1] K. E. Atkinson, *User's Guide to a Boundary Element Package for Solving Integral Equations on Piecewise Smooth Surfaces, Release No. 2*, U. of Iowa, 1998.

[2] K. E. Atkinson, *The Numerical Solution of Integral Equations of the Second Kind,* Cambridge U. Press (1997) ISBN 0-521-58391-8.

k	N	cond(D_N)	cond(S_N)	$\delta = 0$(tsvd)	0(cg)	0.01(tsvd)	0.01(cg)
1	50	2.7	$2.9 \cdot 10^1$	.23(48)	.18(9)	.24(48)	.18(9)
1	194	2.9	$2.7 \cdot 10^2$	.14(143)	.13(19)	.19(103)	.16(15)
1	770	2.9	$2.8 \cdot 10^4$	.048(698)	.047(32)	.096(148)	.089(17)
3	50	9.4	$1.5 \cdot 10^1$	.30(50)	.30(24)	.30(50)	.30(24)
3	194	33.9	$1.0 \cdot 10^2$	.14(141)	.14(27)	.15(126)	.15(24)
3	770	100.	$1.2 \cdot 10^4$	.041(692)	.040(37)	.061(180)	.061(25)
6	50	12.8	$8.4 \cdot 10^1$	.93(33)	.84(2)	.93(33)	.84(2)
6	194	11.3	$2.9 \cdot 10^1$	.34(192)	.34(142)	.35(194)	.35(135)
6	770	29.1	$5.8 \cdot 10^3$	.082(690)	.082(97)	.099(340)	.12(45)

Table 3: Comparison of optimal relative errors using tsvd and cg for Example 2 (cylinder with hemispherical endcaps).

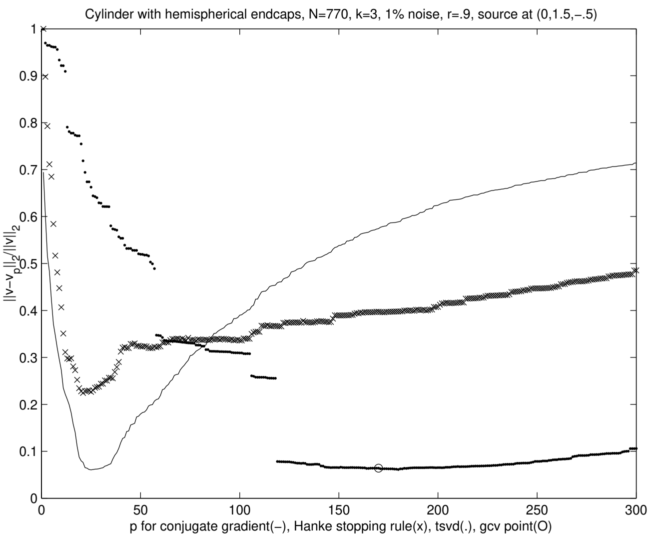

Figure 4.

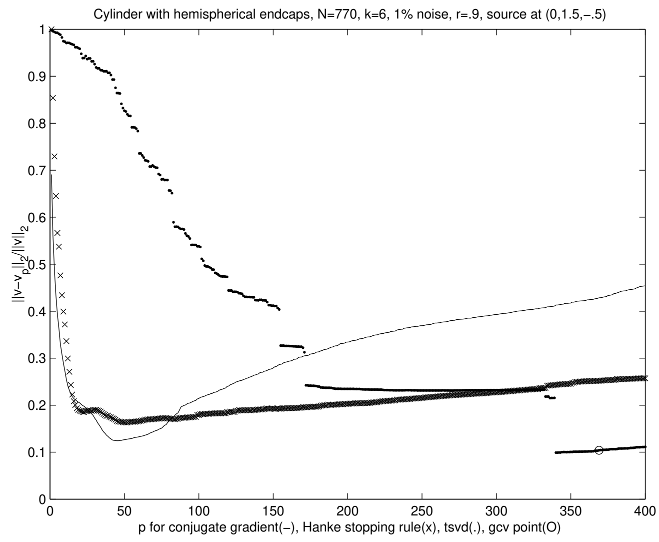

Figure 5.

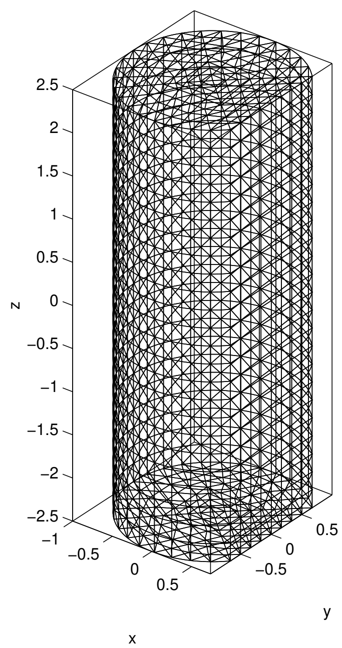

Figure 6. Discretization of Γ into boundary elements for Example 3.

k	N	cond(D_N)	cond(S_N)	$\delta = 0$(tsvd)	0(cg)	0.01(tsvd)	0.01(cg)
1	66	35.6	$1.3 \cdot 10^2$	.45(43)	.42(9)	.45(43)	.43(9)
1	258	29.6	$2.9 \cdot 10^3$	.34(178)	.34(27)	.36(139)	.35(19)
1	1026	34.0	$5.4 \cdot 10^8$	.25(585)	.25(44)	.26(186)	.26(20)
3	66	31.7	$4.0 \cdot 10^1$	.56(63)	.56(38)	.56(62)	.56(35)
3	258	84.6	$1.3 \cdot 10^3$	.37(158)	.37(34)	.37(144)	.37(30)
3	1026	121.	$2.6 \cdot 10^8$	.26(766)	.26(215)	.26(223)	.26(34)
6	66	56.1	$1.0 \cdot 10^2$	.90(45)	.86(1)	.90(45)	.86(1)
6	258	360.	$4.6 \cdot 10^2$	.54(254)	.53(185)	.55(248)	.59(184)
6	1026	182.	$1.0 \cdot 10^8$	.26(801)	.26(230)	.31(608)	.31(74)

Table 4: Comparison of optimal relative 2-norm errors using tsvd and cg for Example 3 (cylinder with flat endcaps and floor).

k	N	cond(D_N)	cond(S_N)	$\delta = 0$(tsvd)	0(cg)	0.01(tsvd)	0.01(cg)
1	66	35.6	$1.3 \cdot 10^2$	.12(64)	.12(9)	.13(60)	.12(9)
1	258	29.6	$2.9 \cdot 10^3$	.063(254)	.061(41)	.093(99)	.079(18)
1	1026	34.0	$5.4 \cdot 10^8$	.030(808)	.030(344)	.055(178)	.047(18)
3	66	31.7	$4.0 \cdot 10^1$	.31(65)	.31(41)	.31(63)	.31(38)
3	258	84.6	$1.3 \cdot 10^3$	.14(256)	.37(34)	.16(159)	.16(33)
3	1026	121.	$2.6 \cdot 10^8$	.064(892)	.064(215)	.094(222)	.094(34)
6	66	56.1	$1.0 \cdot 10^2$	1.42(17)	1.35(1)	1.42(17)	1.35(1)
6	258	360.	$4.6 \cdot 10^2$	.56(256)	.50(206)	.61(256)	.55(125)
6	1026	182.	$1.0 \cdot 10^8$	.15(909)	.15(230)	.37(609)	.37(74)

Table 5: Comparison of optimal average pointwise errors using tsvd and cg for Example 3 (cylinder with flat endcaps and floor).

N	18	66	258	1026
S	5.21	24.63	115.81	841.88
D	15.54	74.76	342.27	2905.99
SVD	0.01	0.45	22.89	1797.56
p by *gcv*	0.11	0.13	0.32	23.53
ϕ by *tsvd*	0.12	0.13	0.35	179.46
$v_p = D * \phi$	0.03	0.02	0.06	35.80

Table 6: Sample timings for the numerical algorithm for Example 3.

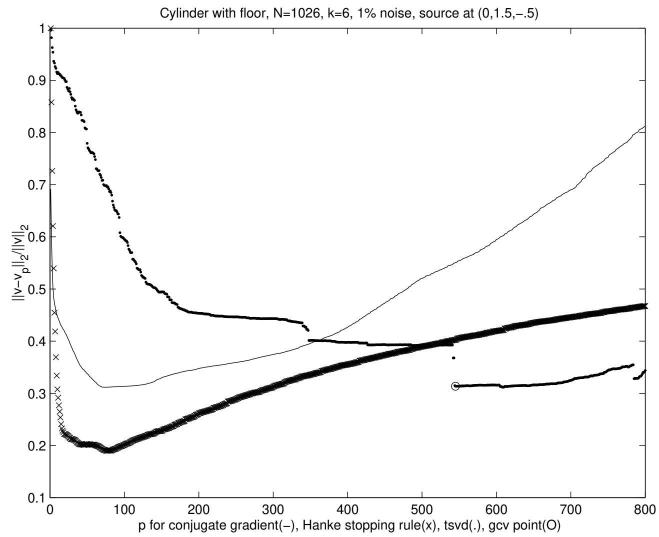

Figure 7.

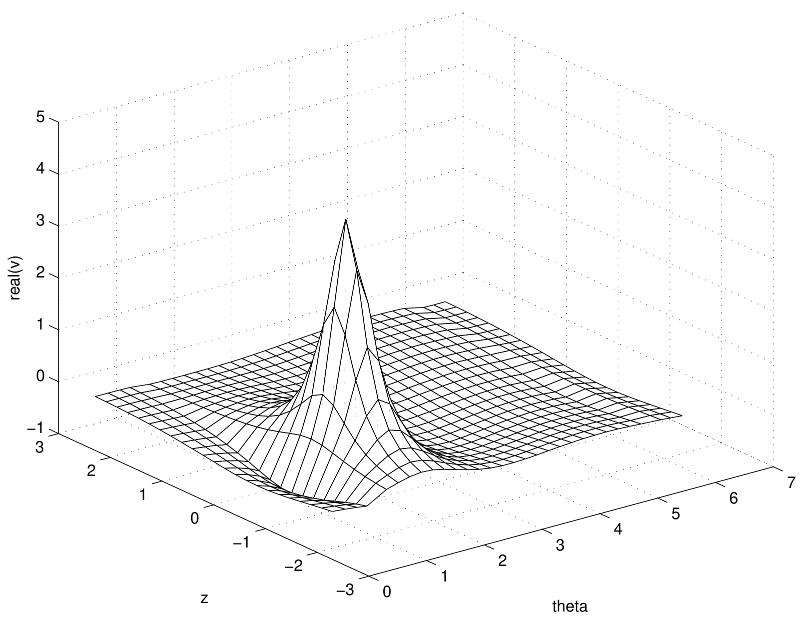

Figure 8. Exact velocity for Example 3.

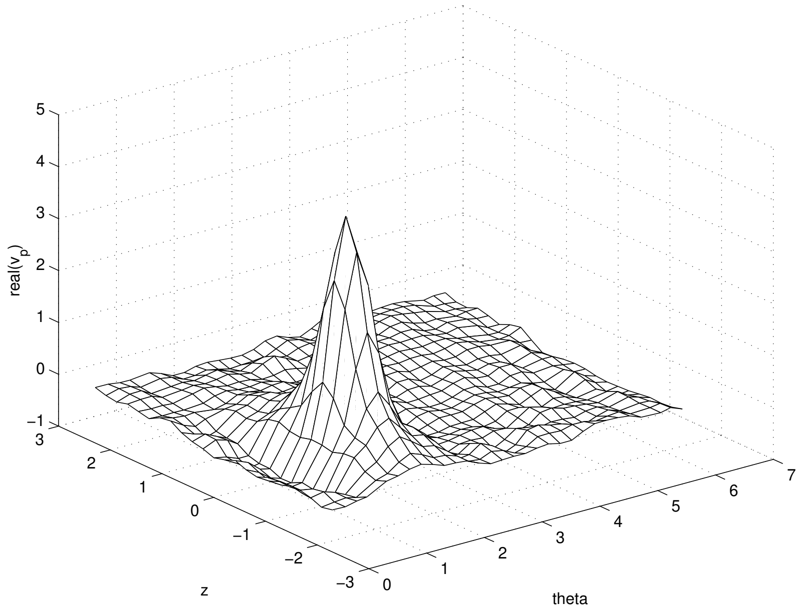

Figure 9. Recovered velocity for Example 3.

[3] D. Colton, R. Kress, *Inverse acoustic and electromagnetic scattering theory*, Springer-Verlag,New York, 1992.

[4] T. DeLillo, V. Isakov, N. Valdivia, L. Wang, *The detection of the source of acoustical noise in two dimensions*, SIAM J. Appl. Math., 66, 6 (2001) 2104–2121.

[5] H. W. Engl, M. Hanke, A. Neubauer, *Regularization of inverse problems*, Kluwer, Dordrecht, 1996.

[6] M. Hanke, *Conjugate gradient type methods for ill-posed problems*, Pitman Research Notes in Mathematics Series 327, Longman Scientific and Technical, Essex, UK, 1995.

[7] P.C. Hansen, *Regularization Tools: A Matlab Package for Analysis and Solution of Discrete Ill-Posed Problems,version 2.0 for Matlab 4.0*,

[8] P. C. Hansen, *Rank-Deficient and Discrete Ill-Posed Problems–Numerical Aspects of Linear Inversion*, SIAM, 1998.

[9] V. Isakov, *Inverse Source Problems*, AMS, Providence, R.I., 1990.

[10] V. Isakov, *Inverse Problems for Partial Differential Equations*, Springer-Verlag, New York, 1998.

[11] V. Isakov, *On detecting the source of Acoustical Noise*, in "Theoretical and Computational Acoustics 2001", World Scientific, 615-629.

[12] V. Isakov, S. Wu, *On theory and applications of the Helmholtz equation least squares method in inverse scattering*, Inverse Problems, 18 (2002), 1141-1161.

[13] M. Kilmer and G. W. Stewart, *Iterative regularization and MINRES*, SIAM J. Matrix Anal. Appl., 21 (1999) 613–628.

[14] R. Kress, *Linear Integral Equations*, Springer-Verlag, New York, 1992.

[15] W. McLean, *Strongly Elliptic Systems and Boundary Integral Euqations*, Cambridge Univ. Press, 2000.

[16] E.G. Williams, *Fourier Acoustics*, Academic Press,New York, 1999

[17] E.G. Williams, B.H. Houston, P. C. Herdic, S. T. Raveendra, and B. Gardner, *Interior near-field acoustical holography in flight*, J. Acoust. Soc. Am. 108 (2000) 1451–1463.